Thermal Stress Analysis of laminated structures by a variable kinematic MITC9 shell element

(Article begins on next page)

02 September 2025

Thermal Stress Analysis of laminated structures by a variable kinematic MITC9 shell element

M. Cinefra[1], S. Valvano[1], E. Carrera[1]

(1) Department of Aeronautics and Space Engineering,
Politecnico di Torino, Turin, Italy

Author and address for Correspondence
Dr. Maria Cinefra
Research Assistant,
Department of Aeronautics and Space Engineering
Politecnico di Torino,
Corso Duca degli Abruzzi, 24,
10129 Torino, ITALY,
tel +39.011.546.6869, fax +39.011.564.6899
e.mail: maria.cinefra@polito.it

Abstract

A linear static thermal stress analysis of composite shell structures is carried out by means of a shell finite element with variable through-the-thickness kinematic. The refined models used are both Equivalent Single Layer (ESL) and Layer Wise (LW) and they are grouped in the Unified Formulation by Carrera (CUF). These models permit the distribution of displacements, stresses and temperature along the thickness of the multi-layered shell to be accurately described. The Principle of Virtual Displacement (PVD) is employed to derive the governing equations. The Mixed Interpolation of Tensorial Components (MITC) method is used to contrast the membrane and shear locking phenomenon for a nine-node shell element. Cross-ply plate, cylindrical and spherical shells with simply-supported edges and subjected to bi-sinusoidal thermal load are analyzed and various thickness ratios are considered. The results, obtained with different theories contained in the CUF, are compared with both the elasticity solutions given in the literature and the analytical solutions obtained using higher-order models and the Navier's method. From the analysis, one can conclude that the shell element based on the CUF is very efficient, and its use leads to reach higher accuracy than classical models in the study of layered structures.

Introduction

An increasing amount of modern aerospace vehicles is made up of composite structures such as multilayered carbon-fiber reinforced and/or sandwich plates and shells. Many of these structures are simultaneously loaded by high thermal and mechanical loads. Consequently the thermal deformations and stresses which are induced by non-uniform temperature in composite structures become important parameters in structural design. Use of higher-order theories will make it possible to determine these parameters precisely

in composite structures. Studies involving the thermo-elastic behaviour using classical or first-order theories are described by Kant and Khare [1] and Khdeir and Reddy [2]. The first ever literature available based on higher-order theory is by Pao [3] who developed higher-order equations applying Flügge's [4] shell theory to orthotropic and laminated materials for the analysis of composite shells under thermal loading. Kant [5, 6] presented a general theory for small deformations of a thick shell made up of a layered system of different orthotropic materials having planes of symmetry coincident with the orthogonal reference frame and subjected to mechanical and arbitrary temperature distribution. Kant and Patil [7, 8] presented the governing equations describing the behaviour of a general shell form, subjected to both mechanical and thermal loads, specifically for two thick shell theories in addition to a so-called thin shell theory. They considered the numerical examples drawn from literature for the analysis of pressure vessels.

In the last few years, several higher-order two-dimensional models have been developed for such problems, which consider only an assumed temperature profile through the thickness. Among these, of particular interest is the higher-order model by Whu and Chen [9], which describes the displacements and stresses in laminated in thermal bending by assuming a linear profile of temperature through the thickness z. The same temperature profile is used by Khare et alii [10] to obtain a closed-form solution for the thermomechanical analysis of laminated and sandwich shells. Khdeir [11] and Khdeir et alii [12] assume a linear or constant temperature profile through the thickness, in the first the thermoelastic governing equations for laminated shells are exactly solved, in the second a Higher Shear Deformation Theory is given. An interesting method to analyze the thermal stresses in shells is the use of Cosserat surfaces, as done by Birsan [13] for two given temperature fields and Iesan [14] for an assumed polynomial temperature variation in the axial coordinate. Barut et alii [15] analyze the non-linear thermoelastic behavior of shells by means of the Finite Element Method, but the assigned temperature

profile is linear. In the framework of the arbitrary distribution of temperature through the thickness, Miller et alii [16] and Dumir et alii [17] are noteworthy, in the first a classical shell theory for composite shells is given, the second remarks the importance of the zig-zag form of displacements in the thermal analysis of composite shells. In the case of shells, further investigations were made by Hsu et alii [18] for both closed form and Finite Element method, and by Ding [19] for a weak formulation for the case of state equations including the boundary conditions. The importance of mechanical and thermal anisotropy in such investigations was remarked by Padovan in [20]. Some interesting experimental results can be found in [21]; Kapuria et alii [22] suggest the use of piezoelectric layers to contrast such thermal deformations.

In the last few years many contributions have been proposed, which are based on Carrera Unified Formulation, to investigate the thermal effects in composite structures. In [23] a study on the influence of the through-the-thickness temperature profile on the thermomechanical response of multilayered anisotropic thick and thin plates has been addressed. The partially coupled stress problem was considered by solving the Fourier's conductivity equation. The importance of mixed theories for a correct prediction of transverse shear/normal stresses due to thermal loadings have been remarked in [24, 25], this is extended also for thermopiezoelastic problems in [26]. A fully coupled thermo-mechanical analysis applied to plate structure is employed in [27]. Different type of loads as problems related to uniform, triangular, bitriangular (tentlike), and localized in-plane distribution of temperature were considered in [28]. The Ritz method, based on the choice of trigonometric trial functions, was used in [29]. Extension to Functionally Graded Materials (FGMs) has been done in [30]. A thermal stability analysis of functionally graded material, isotropic and sandwich plates is studied in [31], the Ritz method is employed and uniform, linear, and non-linear temperature profile is taken into account for different cases. An extension of the thermoelastic formulation to shells has been done in [32]. The thermo-mechanical analysis of functionally graded shell is

4

considered in [33]. Analytical closed form solutions are available in very few cases. The solution of the most of the practical problems demand applications of approximated computational methods.

An improved doubly-curved shell finite element for the analysis of composite structures under thermal loads is here presented, it is a natural extension of the plate finite element presented in [34]. The shell finite element is based on the Carrera's Unified Formulation (CUF), which was developed by Carrera for multi-layered structures [35, 36]. Both Equivalent Single Layer (ESL) and Layer Wise (LW) theories contained in the CUF have been implemented in the shell finite element. The Mixed Interpolation of Tensorial Components (MITC) method [37, 38, 39, 40] is used to contrast the membrane and shear locking. The governing equations for the linear static analysis of composite structures are derived from the Principle of Virtual Displacement (PVD), in order to apply the finite element method. The temperature profile is considered always linear through the thickness for each two-dimensional model, to point out the importance of refined kinematics in the case of multilayered composite shells [41]. Cross-ply plate, cylindrical and spherical shells with simply-supported edges and subjected to bi-sinusoidal thermal loads are analyzed. The results obtained with the different models contained in the CUF, are compared with the exact solution given in the literature and the analytical Navier's solution type. A future companion paper would investigate the effects of the calculated temperature profile for thick and thin multilayered composite shells.

Preliminaries

Shells are bi-dimensional structures in which one dimension (in general the thickness in z direction) is negligible with respect to the other two in-plane dimensions. Geometry and the reference system are indicated in Fig. 1. By considering multilayered structures, the square of an infinitesimal linear segment in the layer, the associated infinitesimal

area and volume are given by:

$$ds_k^2 = \quad H_\alpha^{k^2} \, d\alpha_k^2 \; + \; H_\beta^{k^2} \, d\beta_k^2 + H_z^{k^2} \, dz_k^2$$

$$d\Omega_k = \quad H_\alpha^k H_\beta^k \, d\alpha_k \, d\beta_k \tag{1}$$

$$dV = \quad H_\alpha^k \, H_\beta^k \, H_z^k \, d\alpha_k \, d\beta_k \, dz_k$$

where the metric coefficients are:

$$H_\alpha^k = A^k(1 + z_k/R_\alpha^k), \quad H_\beta^k = B^k(1 + z_k/R_\beta^k), \quad H_z^k = 1 \tag{2}$$

k denotes the k-layer of the multilayered shell; R_α^k and R_β^k are the principal radii of the midsurface of the layer k. A^k and B^k are the coefficients of the first fundamental form of Ω_k (Γ_k is the Ω_k boundary). In this paper, the attention has been restricted to shells with constant radii of curvature (cylindrical, spherical, toroidal geometries) for which $A^k = B^k = 1$. Details for shells are reported in [42].

Geometrical relations permit the in-plane $\boldsymbol{\epsilon}_p^k$ and out-plane $\boldsymbol{\epsilon}_n^k$ strains to be expressed in terms of the displacement $\boldsymbol{u}$. The following relations hold:

$$\boldsymbol{\epsilon}_p^k = [\epsilon_{\alpha\alpha}^k, \epsilon_{\beta\beta}^k, \epsilon_{\alpha\beta}^k]^T = (\boldsymbol{D}_p^k + \boldsymbol{A}_p^k)\, \boldsymbol{u}^k \; , \; \boldsymbol{\epsilon}_n^k = [\epsilon_{\alpha z}^k, \epsilon_{\beta z}^k, \epsilon_{zz}^k]^T = (\boldsymbol{D}_{n\Omega}^k + \boldsymbol{D}_{nz}^k - \boldsymbol{A}_n^k)\, \boldsymbol{u}^k$$
$$\tag{3}$$

The explicit form of the introduced arrays is:

$$\boldsymbol{D}_p^k = \begin{bmatrix} \frac{\partial_\alpha}{H_\alpha^k} & 0 & 0 \\ 0 & \frac{\partial_\beta}{H_\beta^k} & 0 \\ \frac{\partial_\beta}{H_\beta^k} & \frac{\partial_\alpha}{H_\alpha^k} & 0 \end{bmatrix}, \quad \boldsymbol{D}_{n\Omega}^k = \begin{bmatrix} 0 & 0 & \frac{\partial_\alpha}{H_\alpha^k} \\ 0 & 0 & \frac{\partial_\beta}{H_\beta^k} \\ 0 & 0 & 0 \end{bmatrix}, \quad \boldsymbol{D}_{nz}^k = \begin{bmatrix} \partial_z & 0 & 0 \\ 0 & \partial_z & 0 \\ 0 & 0 & \partial_z \end{bmatrix} \tag{4}$$

6

$$\boldsymbol{A}_p^k = \begin{bmatrix} 0 & 0 & \frac{1}{H_\alpha^k R_\alpha^k} \\ 0 & 0 & \frac{1}{H_\beta^k R_\beta^k} \\ 0 & 0 & 0 \end{bmatrix}, \; \boldsymbol{A}_n^k = \begin{bmatrix} \frac{1}{H_\alpha^k R_\alpha^k} & 0 & 0 \\ 0 & \frac{1}{H_\beta^k R_\beta^k} & 0 \\ 0 & 0 & 0 \end{bmatrix} \tag{5}$$

The definition of the 3D constitutive equations permits to express the stresses by means of the strains. The generalized Hooke's law is considered, by employing a linear constitutive model for infinitesimal deformations. In a composite material, these equations are obtained in material coordinates $(1, 2, 3)$ for each orthotropic layer k and then rotated in the general curvilinear reference system (α, β, z). Therefore, the stress-strain relations after the rotation are:

$$\boldsymbol{\sigma}_p^k = \boldsymbol{\sigma}_{pd}^k - \boldsymbol{\sigma}_{pT}^k = \boldsymbol{C}_{pp}^k \, \boldsymbol{\epsilon}_p^k + \boldsymbol{C}_{pn}^k \, \boldsymbol{\epsilon}_n^k - \boldsymbol{\lambda}_p^k \, \theta^k$$
$$\boldsymbol{\sigma}_n^k = \boldsymbol{\sigma}_{nd}^k - \boldsymbol{\sigma}_{nT}^k = \boldsymbol{C}_{np}^k \, \boldsymbol{\epsilon}_p^k + \boldsymbol{C}_{nn}^k \, \boldsymbol{\epsilon}_n^k - \boldsymbol{\lambda}_n^k \, \theta^k \tag{6}$$

where

$$\boldsymbol{C}_{pp}^k = \begin{bmatrix} C_{11}^k & C_{12}^k & C_{16}^k \\ C_{12}^k & C_{22}^k & C_{26}^k \\ C_{16}^k & C_{26}^k & C_{66}^k \end{bmatrix} \qquad \boldsymbol{C}_{pn}^k = \begin{bmatrix} 0 & 0 & C_{13}^k \\ 0 & 0 & C_{23}^k \\ 0 & 0 & C_{36}^k \end{bmatrix}$$

$$\boldsymbol{C}_{np}^k = \begin{bmatrix} 0 & 0 & 0 \\ 0 & 0 & 0 \\ C_{13}^k & C_{23}^k & C_{36}^k \end{bmatrix} \qquad \boldsymbol{C}_{nn}^k = \begin{bmatrix} C_{55}^k & C_{45}^k & 0 \\ C_{45}^k & C_{44}^k & 0 \\ 0 & 0 & C_{33}^k \end{bmatrix} \tag{7}$$

$$\boldsymbol{\lambda}_p^k = \boldsymbol{C}_{pp}^k \, \boldsymbol{\alpha}_p^k + \boldsymbol{C}_{pn}^k \, \boldsymbol{\alpha}_n^k$$
$$\boldsymbol{\lambda}_n^k = \boldsymbol{C}_{np}^k \, \boldsymbol{\alpha}_p^k + \boldsymbol{C}_{nn}^k \, \boldsymbol{\alpha}_n^k \tag{8}$$

$$\boldsymbol{\alpha}_p^k = \begin{bmatrix} \boldsymbol{\alpha}_1^k \\ \boldsymbol{\alpha}_2^k \\ 0 \end{bmatrix} \qquad \boldsymbol{\alpha}_n^k = \begin{bmatrix} 0 \\ 0 \\ \boldsymbol{\alpha}_3^k \end{bmatrix} \tag{9}$$

$$\boldsymbol{\lambda}_p^k = \begin{bmatrix} \boldsymbol{\lambda}_1^k \\ \boldsymbol{\lambda}_2^k \\ \boldsymbol{\lambda}_6^k \end{bmatrix} \qquad \boldsymbol{\lambda}_n^k = \begin{bmatrix} 0 \\ 0 \\ \boldsymbol{\lambda}_3^k \end{bmatrix} \tag{10}$$

The subscripts d and T mean mechanical and thermal contributions. The material coefficients C_{ij} depend on the Young's moduli E_1, E_2, E_3, the shear moduli G_{12}, G_{13}, G_{23} and Poisson moduli ν_{12}, ν_{13}, ν_{23}, ν_{21}, ν_{31}, ν_{32} that characterize the layer material. α_{ij} are the thermal expansion coefficients, λ_{ij} are the coupling thermal coefficients and θ^k is the temperature.

Hierarchical Shell Theories

The variation of the displacement variables along the thickness direction is a-priori postulated. Several displacement-based theories can be formulated on the basis of the following generic kinematic field. The main feature of the Unified Formulation by Carrera [36, 43, 44] (CUF) is the unified manner in which the displacement variables are handled.

$$\boldsymbol{u}^k(\alpha, \beta, z) = F_s(z)\boldsymbol{u}_s^k(\alpha, \beta) \qquad \delta\boldsymbol{u}^k(\alpha, \beta, z) = F_\tau(z)\delta\boldsymbol{u}_\tau^k(\alpha, \beta) \qquad \tau, s = 0, 1, ..., N \tag{11}$$

where (α, β, z) is a curvilinear reference system, in which α and β are orthogonal and the curvature radii R_α and R_β are constant in each point of the domain Ω (see Fig. 1). The displacement vector $\boldsymbol{u} = \{u, v, w\}$ has its components expressed in this system. $\delta\boldsymbol{u}$

indicates the virtual displacement associated to the virtual work and k identifies the layer. F_τ and F_s are the so-called thickness functions depending only on z. $\boldsymbol{u}_s$ are the unknown variables depending on the coordinates α and β. τ and s are sum indexes and N is the order of expansion in the thickness direction assumed for the displacements.

Classical Theories

The simplest plate/shell theory is based on the Kirchoff/Love's hypothesis, and it is usually referred to as Classical Lamination Theory (CLT)[45],[46]. Both transverse shear strains and transverse normal strains are discarded, in usual applications being negligible with respect to the in-plane ones,

$$
\begin{cases}
u(x,y,z) = u_0(x,y) - z\dfrac{\partial w_0}{\partial x} \\[2mm]
v(x,y,z) = v_0(x,y) - z\dfrac{\partial w_0}{\partial y} \\[2mm]
w(x,y,z) = w_0(x,y)
\end{cases}
\tag{12}
$$

The inclusion of transverse shear strains, in the theory mentioned here, leads to Reissner-Mindlin Theory, also known as First-order Shear Deformation Theory (FSDT) [47],

$$
\begin{cases}
u(x,y,z) = u_0(x,y) + z\,u_1(x,y) \\[2mm]
v(x,y,z) = v_0(x,y) + z\,v_1(x,y) \\[2mm]
w(x,y,z) = w_0(x,y)
\end{cases}
\tag{13}
$$

However, these theories, due to their inconsistency in discarding the transverse normal stress in the material constitutive equations, are no longer valid when 3D local effects appear. To remove the inconsistency completely, higher-order expansion of the unknowns with respect to the z coordinate are needed.

Refined Theories

Many attempts have been made to improve classical plate/shell models. The CUF has the capability to expand each displacement variable in the displacement field at any desired order independently from the others and with respect to the accuracy and the computational cost has been introduced. Such an artifice permits each variable to be handled independently from the others. This becomes extremely useful when multifield problems are investigated such as thermoelastic and piezoelectric applications [24, 32, 48].

In the case of Equivalent Single Layer (ESL) models, a Taylor expansion is employed as thickness functions:

$$\boldsymbol{u} = F_0\,\boldsymbol{u}_0 + F_1\,\boldsymbol{u}_1 + \ldots + F_N\,\boldsymbol{u}_N = F_s\,\boldsymbol{u}_s, \qquad s = 0, 1, \ldots, N \tag{14}$$

$$F_0 = z^0 = 1, \quad F_1 = z^1 = z, \quad \ldots, \quad F_N = z^N. \tag{15}$$

Following this approach the displacement field can be written as:

$$\begin{cases} u(x,y,z) = u_0(x,y) + z\,u_1(x,y) + \ldots + z^N\,u_N(x,y) \\[2mm] v(x,y,z) = v_0(x,y) + z\,v_1(x,y) + \ldots + z^N\,v_N(x,y) \\[2mm] w(x,y,z) = w_0(x,y) + z\,w_1(x,y) + \ldots + z^N\,w_N(x,y) \end{cases} \tag{16}$$

In general:

$$\begin{cases} u(x,y,z) = F_0(x,y) + F_1\,u_1(x,y) + \ldots + F_N\,u_N(x,y) \\[2mm] v(x,y,z) = F_0(x,y) + F_1\,v_1(x,y) + \ldots + F_N\,v_N(x,y) \\[2mm] w(x,y,z) = F_0(x,y) + F_1\,w_1(x,y) + \ldots + F_N\,w_N(x,y) \end{cases} \tag{17}$$

Classical models, such as those based on the First-order Shear Deformation Theory (FSDT), can be obtained from an ESL theory with $N = 1$, by imposing a constant transverse displacement through the thickness via penalty techniques. Also a model based on the hypotheses of Classical Lamination Theory (CLT) can be expressed by means of the CUF by applying a penalty technique to the constitutive equations (see section). This permits to impose that the transverse shear strains are null in the shell.

Advanced Theories

Due to the intrinsic anisotropy of multilayered structures, the first derivative of the displacement variables in the z-direction is discontinuous. The Layer-Wise (LW) models, in respect to the ESLs, allow the zig-zag form of the displacement distribution in layered structures to be modelled. It is possible to reproduce the zig-zag effects also in the framework of the ESL description by employing the Murakami theory. According to references [49], a zig-zag term can be introduced into equation(14) as follows:

$$\boldsymbol{u}^k = F_0 \, \boldsymbol{u}_0^k + \ldots + F_N \, \boldsymbol{u}_N^k + (-1)^k \zeta_k \boldsymbol{u}_Z^k \qquad (18)$$

Subscript Z refers to the introduced term. Such theories are called zig-zag (Z) theories. Following this approach the displacement field can be written as:

$$\begin{cases} u(x,y,z) = F_0(x,y) + F_1 \, u_1(x,y) + \ldots + F_{N-1} \, u_{N-1}(x,y) + (-1)^k \zeta_k u_{Z_N}^k \\[2mm] v(x,y,z) = F_0(x,y) + F_1 \, v_1(x,y) + \ldots + F_{N-1} \, v_{N-1}(x,y) + (-1)^k \zeta_k v_{Z_N}^k \\[2mm] w(x,y,z) = F_0(x,y) + F_1 \, w_1(x,y) + \ldots + F_{N-1} \, w_{N-1}(x,y) + (-1)^k \zeta_k w_{Z_N}^k \end{cases} \qquad (19)$$

In the case of Layer-Wise (LW) models, the displacement is defined at k-layer level:

$$\boldsymbol{u}^k = F_t \, \boldsymbol{u}_t^k + F_b \, \boldsymbol{u}_b^k + F_r \, \boldsymbol{u}_r^k = F_s \, \boldsymbol{u}_s^k, \qquad s = t, b, r \; , \quad r = 2, ..., N \qquad (20)$$

$$F_t = \frac{P_0 + P_1}{2}, \quad F_b = \frac{P_0 - P_1}{2}, \quad F_r = P_r - P_{r-2} \qquad (21)$$

in which $P_j = P_j(\zeta_k)$ is the Legendre polynomial of j-order defined in the ζ_k-domain: $-1 \leq \zeta_k \leq 1$. $P_0 = 1$, $P_1 = \zeta_k$, $P_2 = (3\zeta_k^2 - 1)/2$, $P_3 = (5\zeta_k^3 - 3\zeta_k)/2$, $P_4 = (35\zeta_k^4 - 30\zeta_k^2 + 3)/8$. The top (t) and bottom (b) values of the displacements are used as unknown variables and one can impose the following compatibility conditions:

$$u_t^k = u_b^{k+1}, \qquad k = 1, N_l - 1 \qquad (22)$$

Finite Element approximation

In this section, the derivation of a shell finite element for the analysis of multilayered structures is presented. The element is based on both the ESL and LW theories contained in the Unified Formulation. After an overview in scientific literature about the methods that permit to withstand the membrane and shear locking, the MITC technique has been adopted for this element. Considering a 9-nodes finite element with doubly-curved geometry, the displacement components are interpolated on the nodes of the element by means of the Lagrangian shape functions N_i:

$$\boldsymbol{u}_s = N_j \boldsymbol{u}_{s_j} \qquad \delta \boldsymbol{u}_\tau = N_i \delta \boldsymbol{u}_{\tau_i} \qquad \text{with} \quad i, j = 1, ..., 9 \qquad (23)$$

where $\boldsymbol{u}_{s_j}$ and $\delta \boldsymbol{u}_{\tau_i}$ are the nodal displacements and their virtual variations. Substituting in the geometrical relations (3) one has:

$$\epsilon_p = F_\tau(\boldsymbol{D}_p + \boldsymbol{A}_p)(N_i\boldsymbol{I})\boldsymbol{u}_{\tau_i}$$

$$\epsilon_n = F_\tau(\boldsymbol{D}_{n\Omega} - \boldsymbol{A}_n)(N_i\boldsymbol{I})\boldsymbol{u}_{\tau_i} + F_{\tau,z}(N_i\boldsymbol{I})\boldsymbol{u}_{\tau_i}$$

(24)

where $\boldsymbol{I}$ is the identity matrix.

Considering the local coordinate system (ξ, η), the MITC shell elements ([50]-[51]) are formulated by using, instead of the strain components directly computed from the displacements, an interpolation of these within each element using a specific interpolation strategy for each component. The corresponding interpolation points, called *tying points*, are shown in Fig. 4 for a nine-nodes element. Note that the transverse normal strain ϵ_{zz} is excluded from this procedure and it is directly calculated from the displacements. The interpolating functions are Lagrangian functions and are arranged in the following arrays:

$$N_{m1} = [N_{A1}, N_{B1}, N_{C1}, N_{D1}, N_{E1}, N_{F1}]$$

$$N_{m2} = [N_{A2}, N_{B2}, N_{C2}, N_{D2}, N_{E2}, N_{F2}]$$

$$N_{m3} = [N_P, N_Q, N_R, N_S]$$

(25)

From this point on, the subscripts $m1$, $m2$ and $m3$ indicate quantities calculated in the points $(A1, B1, C1, D1, E1, F1)$, $(A2, B2, C2, D2, E2, F2)$ and (P, Q, R, S), respectively. Therefore, the strain components are interpolated as follows:

$$\boldsymbol{\epsilon}_p = \begin{bmatrix} \epsilon_{\alpha\alpha} \\ \epsilon_{\beta\beta} \\ \epsilon_{\alpha\beta} \end{bmatrix} = \begin{bmatrix} N_{m1} & 0 & 0 \\ 0 & N_{m2} & 0 \\ 0 & 0 & N_{m3} \end{bmatrix} \begin{bmatrix} \epsilon_{\alpha\alpha_{m1}} \\ \epsilon_{\beta\beta_{m2}} \\ \epsilon_{\alpha\beta_{m3}} \end{bmatrix}$$

$$\boldsymbol{\epsilon}_n = \begin{bmatrix} \epsilon_{\alpha z} \\ \epsilon_{\beta z} \\ \epsilon_{zz} \end{bmatrix} = \begin{bmatrix} N_{m1} & 0 & 0 \\ 0 & N_{m2} & 0 \\ 0 & 0 & 1 \end{bmatrix} \begin{bmatrix} \epsilon_{\alpha z_{m1}} \\ \epsilon_{\beta z_{m2}} \\ \epsilon_{zz} \end{bmatrix} \tag{26}$$

where the strains $\epsilon_{\alpha\alpha_{m1}}$, $\epsilon_{\beta\beta_{m2}}$, $\epsilon_{\alpha\beta_{m3}}$, $\epsilon_{\alpha z_{m1}}$, $\epsilon_{\beta z_{m2}}$ are expressed by means of eq.s (24) in which the shape functions N_i and their derivatives are evaluated in the tying points. For example, one can considers the strain component $\epsilon_{\alpha\alpha}$ that is calculated as follows:

$$\epsilon_{\alpha\alpha} = N_{A1}\epsilon_{\alpha\alpha_{A1}} + N_{B1}\epsilon_{\alpha\alpha_{B1}} + N_{C1}\epsilon_{\alpha\alpha_{C1}} + N_{D1}\epsilon_{\alpha\alpha_{D1}} + N_{E1}\epsilon_{\alpha\alpha_{E1}} + N_{F1}\epsilon_{\alpha\alpha_{F1}} \tag{27}$$

with:

$$\epsilon_{\alpha\alpha_{A1}} = N_{i,\alpha}^{(A1)} F_\tau u_{\tau_i} + \frac{1}{H_\alpha R_\alpha} N_i^{(A1)} F_\tau w_{\tau_i} \tag{28}$$

The superscript $(A1)$ indicates that the shape function and its derivative are evaluated in the point of coordinates $(-\frac{1}{\sqrt{3}}, -\sqrt{\frac{3}{5}})$. Similar expressions can be written for $\epsilon_{\alpha\alpha_{B1}}, \epsilon_{\alpha\alpha_{C1}}, \epsilon_{\alpha\alpha_{D1}}, \epsilon_{\alpha\alpha_{E1}}, \epsilon_{\alpha\alpha_{F1}}$.

Governing FEM equations

The PVD for a multilayered doubly-curved shell reads:

$$\int\limits_{\Omega_k}\int\limits_{A_k} \left\{ \delta\boldsymbol{\epsilon}_p^{kT}\boldsymbol{\sigma}_p^k + \delta\boldsymbol{\epsilon}_n^{kT}\boldsymbol{\sigma}_n^k \right\} H_\alpha^k H_\beta^k \, d\Omega_k dz = \delta L_e \tag{29}$$

where Ω_k and A_k are the integration domains in the plane and in the thickness direction, respectively. The left hand side of the equation represents the variation of the internal work, while the right hand side is the external work. $\boldsymbol{\sigma}_p^k$ and $\boldsymbol{\sigma}_n^k$ contain the mechanical (d) and thermal (T) contributions, so:

$$\int\limits_{\Omega_k}\int\limits_{A_k} \left\{ \delta\boldsymbol{\epsilon}_p^{kT}\left(\boldsymbol{\sigma}_{pd}^k - \boldsymbol{\sigma}_{pT}^k\right) + \delta\boldsymbol{\epsilon}_n^{kT}\left(\boldsymbol{\sigma}_{nd}^k - \boldsymbol{\sigma}_{nT}^k\right) \right\} H_\alpha^k H_\beta^k \, d\Omega_k dz = \delta L_e \tag{30}$$

In this work no mechanical loads are applied to the shell structure, so the external work is null, except for the thermal stress contribution of the temperature distribution applied, so:

$$\int\limits_{\Omega_k}\int\limits_{A_k} \left\{ \delta\boldsymbol{\epsilon}_p^{kT}\boldsymbol{\sigma}_{pd}^k + \delta\boldsymbol{\epsilon}_n^{kT}\boldsymbol{\sigma}_{nd}^k \right\} H_\alpha^k H_\beta^k \, d\Omega_k dz = \int\limits_{\Omega_k}\int\limits_{A_k} \left\{ \delta\boldsymbol{\epsilon}_p^{kT}\boldsymbol{\sigma}_{pT}^k + \delta\boldsymbol{\epsilon}_n^{kT}\boldsymbol{\sigma}_{nT}^k \right\} H_\alpha^k H_\beta^k \, d\Omega_k dz$$

$$\tag{31}$$

Substituting the constitutive equations (6), the geometrical relations written via the MITC method (26) and applying the Unified Formulation (11) and the FEM approximation (23), one obtains the following governing equations:

$$\delta\boldsymbol{q}_u^{k\tau i}: \quad \boldsymbol{K}_{uu}^{k\tau sij}\boldsymbol{q}_u^{ksj} = \boldsymbol{K}_{u\theta}^{k\tau i}\boldsymbol{q}_{u\theta}^{k\tau i} \tag{32}$$

where $\boldsymbol{K}_{uu}^{k\tau sij}$ is a 3×3 matrix, called fundamental nucleus of the mechanical stiffness matrix, and its explicit expression is given in [52]. This is the basic element from which the stiffness matrix of the whole structure is computed. The fundamental nucleus is

expanded on the indexes τ and s in order to obtain the stiffness matrix of each layer. Then, the matrices of each layer are assembled at multi-layer level depending on the approach considered, ESL or LW. $\boldsymbol{K}_{u\theta}^{k\tau i}$ is a 3×1 matrix, called fundamental nucleus of the thermal load, and its explicit expression is:

$$\boldsymbol{K}_{u\theta_\alpha}^{k\tau i} = \lambda_6^k \, J_\alpha^{k\tau} \, W_{i,\beta}^k + \lambda_1^k \, J_\beta^{k\tau} \, W_{i,\alpha}^k \tag{33}$$

$$\boldsymbol{K}_{u\theta_\beta}^{k\tau i} = \lambda_2^k \, J_\alpha^{k\tau} \, W_{i,\beta}^k + \lambda_6^k \, J_\beta^{k\tau} \, W_{i,\alpha}^k \tag{34}$$

$$\boldsymbol{K}_{u\theta_z}^{k\tau i} = \lambda_3^k \, J_{\alpha\beta}^{k\tau,z} \, W_i^k + \frac{\lambda_2^k}{R_\beta^k} \, J_\alpha^{k\tau} \, W_i^k + \frac{\lambda_1^k}{R_\alpha^k} \, J_\beta^{k\tau} \, W_i^k \tag{35}$$

Where the following integrals in the domain Ω_k are defined:

$$\left(W_i^k \, ; \, W_{i,\alpha}^k \, ; \, W_{i,\beta}^k \right) = \int_{\Omega_k} \left(N_i \, ; \, \frac{\partial N_i}{\partial \alpha} \, ; \, \frac{\partial N_i}{\partial \beta} \right) d\alpha_k d\beta_k \tag{36}$$

Moreover, the integrals on the domain A_k, in the thickness direction, are written as:

$$\left(J_\alpha^{k\tau} ; J_\beta^{k\tau} ; J_{\alpha\beta}^{k\tau,z} \right) = \int_{A_k} \left(F_\tau H_\alpha^k \, ; \, F_\tau H_\beta^k \, ; \, \frac{\partial F_\tau}{\partial z} H_\alpha^k H_\beta^k \right) dz \tag{37}$$

$\boldsymbol{q}_u^{ksj}$, $\delta\boldsymbol{q}_u^{k\tau i}$ and $\boldsymbol{q}_{u\theta}^{k\tau i}$ are the nodal displacements, nodal variation displacements and nodal temperatures respectively.

16

Acronyms

Several refined and advanced two-dimensional models are contained in the Unified For-
mulation. Depending on the variables description (LW, ESL) and the order of expansion
N of the displacements in z, a large variety of kinematics shell theories can be obtained.
A system of acronyms is given in order to denote these models. The first letters indicate
the multi-layer approach which can be Equivalent Single Layer (ESL) or Layer Wise
(LW). The number N indicates the order of expansion used in the thickness direction
(from 1 to 4). In the case of LW approach, the same order of expansion is used for
each layer. In the case of ESL approach, a letter Z can be added if the zig-zag effects
of displacements is considered by means of Murakami's zig-zag function. Summarizing,
ESL1-ESL4 are ESL models. If Murakami zig-zag function is used, these equivalent
single layer models are indicated as ESLZ1-ESLZ3. In the case of layer wise approaches,
the letters LW is considered in place of ESL, so the acronyms are LW1-LW4. Sometimes
the Navier analytical method is employed instead of the FEM method and a subscript
(a) is used. Classical theories such as Classical Lamination Theory (CLT) and First
order Shear Deformation Theory (FSDT), can be obtained as particular cases of ESL1
theory simply imposing constant value of w through the thickness direction.

Numerical results

To assess the robustness of this shell element three reference problems are considered:
the first is a cross-ply square multilayered plate with lamination ($0°/90°/0°$) and simply-
supported boundary conditions, compared with the ones obtained with the 3D elasticity
approach by Bhaskar et al. [53]. The second is a cylindrical panel, analytically analyzed,
with three different layout configurations: 1 isotropic layer of Aluminium, 2 isotropic
layers of Titanium and Aluminium, 2 composite layers with lamination ($0°/90°$). The
third is a square, spherical panel, analytically analyzed, made of 2 composite layers with

lamination $(0°/90°)$. The boundary condition is simply-supported. Both of them are evaluated applying a temperature distribution with a bi-sinusoidal in-plane behavior:

$$\theta\left(\alpha, \beta, z\right) = \hat{\theta}\left(z\right) \, sin\left(\frac{m\pi\alpha}{a}\right) sin\left(\frac{n\pi\beta}{b}\right) \tag{38}$$

where $m = n = 1$ and an assumed linear behavior through the thickness:

$$\hat{\theta}\left(z\right) = \theta_{bottom} + \frac{\theta_{top} - \theta_{bottom}}{h} * \left(z + \frac{h}{2}\right) \qquad z \in \left[\frac{-h}{2}\, ; \frac{h}{2}\right] \tag{39}$$

The three problems are briefly described in the following sections.

Multilayered plate

The structure analyzed by Bhaskar et al. [53] (see Figure 3) is a composite multilayered square plate with lamination $(0°/90°/0°)$. The physical properties of the material of the plate, composite, are given in Table 1. The geometrical dimensions are: $a = b = 1.0$. The temperature boundary conditions are: $\theta_{top} = +1.0$, $\theta_{bottom} = -1.0$. The results are presented for different thickness ratios $a/h = 2, 10, 50, 100$. A mesh grid of 10×10 elements is taken to ensure the convergence of the solution. For brevity reasons, the convergence study is here omitted because the robustness of the element was already demonstrated in previous works [54, 55, 52] regarding the mechanical analysis of layered structures. In this case, the thermal load is equivalent to the mechanical load because an uncoupled thermal problem is considered.

The values of the transversal displacement w, the principal in-plane stress $\sigma_{\alpha\alpha}$ and the transverse shear stress $\sigma_{\alpha z}$ are listed in Table 2 for the assumed linear temperature profile. Other results in terms of transverse shear stress and transverse normal stress are shown in Figures 5-8. All the FEs lead to accurate results with respect to the $3D$ [53] and analytical solutions for all the thickness ratios except for $FSDT$. In fact, plate elements that present a constant transverse normal strain such as $FSDT$ lead to inaccurate results

18

for both thick and thin plates. It is confirmed what found in [23]: at least a parabolic expansion for the displacements (u, v, w) is required to capture the linear thermal strains that are related to a linear through-the-thickness temperature distribution. In general, LW theories work better than ESLZ theories, and these last perform better than ESL ones and often also with a lower-order expansion of the unknowns. Equivalent single layer analyses are quite satisfactory only for the transverse displacement or in-plane stresses if applied to thin plates $a/h = 100$, but not for the solution of the transverse normal and shear stresses, as shown in Figures 5-8. On the other hand, higher-order theories lead to better results but computationally more expensive.

The same structure is analyzed with a thermal load with the same bi-sinusoidal in-plane behavior and a constant temperature profile $\hat{\theta}(z) = +1.0$. The results are presented for different thickness ratios $a/h = 10, 100$. The values of the transversal displacement w, the principal in-plane stress $\sigma_{\alpha\alpha}$, the transverse shear stress $\sigma_{\alpha z}$ and the transverse normal stress σ_{zz} are listed in Table 3 for the constant temperature profile case.

Multilayered cylindrical panel

In this section, a cylindrical panel is analysed (see Figure 2). Three different layout configuration are considered:

- 1 layered isotropic cylindrical panel made of Aluminium.

- 2 layered isotropic cylindrical panel made of Titanium and Aluminium.

- 2 layered composite cylindrical panel with lamination $(0°/90°)$.

The temperature boundary conditions are: $\theta_{top} = +0.5$, $\theta_{bottom} = -0.5$ for all the cases. The results are compared with the correspondent closed form solution. A mesh grid of 10×10 elements is taken to ensure the convergence of the solution.

For the 1 and 2 layered isotropic cylindrical panel the geometrical dimensions are: $a = 1.0$ and $b = \dfrac{\pi}{3} R_\beta = 10.47197551$, curvature radii $R_\alpha = \infty$ and $R_\beta = 10$. The results are

presented for different radius to thickness ratios $R_\beta/h_{tot} = (4\,;10\,;100\,;1000)$ with the corresponding thicknesses $h_{tot} = (2.5\,;1.0\,;0.1\,;0.01)$. For the 2 layered isotropic case the bottom layer is made of Aluminium and the top layer is made of Titanium. The physical properties of the Aluminium and Titanium are given in Table 1. The values of the transversal displacement w are listed in Table 4 for the assumed linear temperature profile. All the FEs lead to accurate results with respect to the analytical solutions for all the thickness ratios except for $LW1$, $ESL1$, $FSDT$ elements. For the 2 layered composite cylindrical panel the geometrical dimensions are: $a = 1.0$ and $b = 1.0$, global thickness $h_{tot} = 0.1$, curvature radius $R_\alpha = \infty$. The physical properties of the Carbon are given in Table 1. The results are presented for different radius to thickness ratios $R_\beta/h_{tot} = (10\,;50\,;100\,;500)$ with the corresponding curvature radius $R_\beta = (1.0\,;5.0\,;10.0\,;50.0)$. The lamination angle is $0°$ for the bottom layer and $90°$ for the top layer. The values of the transversal displacement w, the principal in-plane stress $\sigma_{\alpha\alpha}$, the transverse shear stress $\sigma_{\alpha z}$ and the transverse normal stress σ_{zz} are listed in Table 5 for the assumed linear temperature profile. Other results in terms of transverse shear stress and transverse normal stress are shown in Figures 9-12. All the FEs lead to accurate results with respect to the analytical solutions for all the thickness ratios except for $FSDT$ elements. In general, LW theories work better than ESLZ theories, and these last perform better than ESL ones, also when lower orders of expansion are considered. Equivalent single layer analyses are quite satisfactory only for the transverse displacement also for lower radii to thickness ratios $R/h = 10$, but not for the solutions of the stresses, as shown in Figures 9-12.

The same composite cylindrical panel is analyzed with a thermal load with the same bi-sinusoidal in-plane behavior and a constant temperature profile $\hat{\theta}(z) = 0.5$. The results are presented for different thickness ratios $R/h = 10, 100$. The values of the transversal displacement w, the principal in-plane stress $\sigma_{\alpha\alpha}$, the transverse shear stress $\sigma_{\alpha z}$ and the transverse normal stress σ_{zz} are listed in Table 3 for the constant temperature profile

case.

Multilayered spherical panel

In this section, a square, spherical panel is analysed (see Figure 1). The temperature boundary conditions are: $\theta_{top} = +0.5$, $\theta_{bottom} = -0.5$ for all the cases. The results are compared with an analytical solution. A mesh grid of 10×10 elements is taken to ensure the convergence of the solution. The geometrical dimensions are: $a = 1.0$ and $b = 1.0$, global thickness $h_{tot} = 0.1$, curvature radii $R_{\alpha} = R_{\beta} = R$. The physical properties of the Carbon are given in Table 1. The results are presented for different radius to thickness ratios $R/h_{tot} = (10\,;\,50\,;\,100\,;\,500)$ with the corresponding curvature radius $R = (1.0\,;\,5.0\,;\,10.0\,;\,50.0)$. The lamination angle is $0°$ for the bottom layer and $90°$ for the top layer. The values of the transversal displacement w, the principal in-plane stress $\sigma_{\alpha\alpha}$, the transverse shear stress $\sigma_{\alpha z}$ and the transverse normal stress σ_{zz} are listed in Table 6 for the assumed linear temperature profile. Other results in terms of transverse shear stress and transverse normal stress are shown in Figures 13-16. All the FEs lead to accurate results with respect to the analytical solutions for all the thickness ratios except for $FSDT$ elements. In general, LW theories work better than ESLZ theories, and these last perform better than ESL ones and often also with a lower-order expansion of the unknowns. Equivalent single layer analyses are quite satisfactory only for the transverse displacement also for lower radii to thickness ratios $R/h = 10$, but not for the solutions of the stresses, as shown in Figures 13-16.

The same composite spherical panel is analyzed with a thermal load with the same bi-sinusoidal in-plane behavior and a constant temperature profile $\hat{\theta}(z) = 0.5$. The results are presented for different thickness ratios $R/h = 10, 100$. The values of the transversal displacement w, the principal in-plane stress $\sigma_{\alpha\alpha}$, the transverse shear stress $\sigma_{\alpha z}$ and the transverse normal stress σ_{zz} are listed in Table 3 for the constant temperature profile case.

Conclusions

This paper has dealt with the static analysis of composite shells by means of a finite element based on the Unified Formulation by Carrera. The element has been assessed by analyzing cross-ply plates, cylindrical and spherical shells under bi-sinusoidal thermal load with assumed linear temperature profile e few cases with a constant temperature profile, and simply-supported boundary conditions. The results have been presented in terms of both transversal displacement, in-plane stresses and transverse shear stresses, for various thickness ratios and curvature ratios. The performances of the shell element have been tested, and the different theories (classical and refined) contained in the CUF have been compared. The conclusions that can be drawn are the following:

1. The shell element is locking free, for all the LW and ESL considered cases. The results converge to the reference solution by increasing the order of expansion of the displacements in the thickness direction.

2. LW models work better than ESLZ theories, and these last perform better than ESL models in thick shell geometry cases.

3. The classical models, such as FSDT could lead to any inaccurate results.

4. The use of LW models leads to a better accuracy for both thick and thin shells. Their use becomes mandatory if the distribution of transverse stresses in the thickness and the fullfillment of interlaminar continuity conditions are requested.

References

[1] T. Kant and R. K. Khare, Finite element thermal stress analysis of composite laminates using a higher-order theory, *Journal of Thermal Stresses*, vol. 17(2), pp. 229–255, 1994.

[2] A. A. Khdeir and J. N. Reddy, Thermal stresses and deflections of cross-ply laminated plates using refined plate theories, *Journal of Thermal Stresses*, vol. 14(4), pp. 419–438, 1991.

[3] Y. C. Pao, On higher-order theory for thermoelastic analysis of heterogeneous orthotropic cylindrical shells, *Southeastern Conference on Theoretical and Applied Mechanics, 6 th, Tampa, Fla*, pp. 787–806, 1972.

[4] W. Flügge, *Stresses in shells*, Sringer-Verlag, Berlino, 1960.

[5] T. Kant, *Thermal stresses in non-homogeneous shells of revolution: Theory and analysis*, Tech. Rep. IIT-B/CE-79-2, Dept. of Civil Engineering, Indian Institute of Technology, Bombay, 1979.

[6] T. Kant, Thermoelasticity of thick, laminated orthotropic shells, *Proceedings of International Conference on Structural Mechanics in Reactor Technology: Vol. M: Methods for Structural Analysis*, p. 1000, 1981.

[7] T. Kant and S. Patil, *Numerical results-analysis of pressures vessels using various shell theories*, Tech. Rep. Numerical Analysis of Pressure Vessels using Various Shell Theories, Dept. of Civil Engineering, Indian Institute of Technology, Bombay , pp. 149–331, 1979.

[8] T. Kant, *Numerical analysis of pressure vessels using various shell theories*, Tech. Rep. IIT-B/CE-79-1, Dept. of Civil Engineering, Indian Institute of Technology, Bombay, 1979.

[9] W. Zhen and C. Wanji, A global-local higher order theory for multilayered shells and the analysis of laminated cylindrical shell panels, *Composite Structures*, vol. 84(4), pp. 350–361, 2008.

[10] R. K. Khare, T. Kant, and A. K. Garg, Closed-form thermo-mechanical solutions of higher-order theories of cross-ply laminated shallow shells, *Composite Structures*, vol. 59(3), pp. 313–340, 2003.

[11] A. A. Khdeir, Thermoelastic analysis of cross-ply laminated circular cylindrical shells, *International Journal of Solids and Structures*, vol. 33(27), pp. 4007–4017, 1996.

[12] A. A. Khdeir, M. D. Rajab, and J. N. Reddy, Thermal effects on the response of cross-ply laminated shallow shells, *International Journal of Solids and Structures*, vol. 29(5), pp. 653–667, 1992.

[13] M. Bîrsan, Thermal stresses in cylindrical Cosserat elastic shells, *European Journal of Mechanics, A/Solids*, vol. 28(1), pp. 94–101, 2009.

[14] D. Iesan, Thermal stresses in heterogeneous anisotropic cosserat elastic cylinders, *Journal of Thermal Stresses*, vol. 8(4), pp. 385–397, 1985.

[15] A. Barut, E. Madenci and A. Tessler, Nonlinear thermoelastic analysis of composite panels under non-uniform temperature distribution, *International Journal of Solids and Structures*, vol. 37(27), pp. 3681–3713, 2000.

[16] C. J. Miller, W. A. Millavec and T. P. Richer, Thermal stress analysis of layered cylindrical shells, *AIAA J.*, vol. 19(4), pp. 523–530, 1981.

[17] P. C. Dumir, J. K. Nath, P. Kumari and S. Kapuria, Improved efficient zigzag and third order theories for circular cylindrical shells under thermal loading, *Journal of Thermal Stresses*, vol. 31(4), pp. 343–367, 2008.

[18] Y. S. Hsu, J. N. Reddy and C. W. Bert, Thermoelasticity of circular cylindrical shells laminated of bimodulus composite materials, *Journal of Thermal Stresses*, vol. 4(2), pp. 155–177, 1981.

[19] K. Ding, Thermal stresses of weak formulation study for thick open laminated shell, *Journal of Thermal Stresses*, vol. 31(4), pp. 389–400, 2008.

[20] J. Padovan. Thermoelasticity of cylindrically anisotropic generally laminated cylinders, *Journal of Applied Mechanics*, vol. 43(1), pp. 124–130, 1976.

[21] D. Holstein, P. Aswendt, R. Höfling, C. Schmidt and W. Jüptner, Deformation analysis of thermally loaded composite tubes, *Composite Structures*, vol. 40(3-4), pp. 257–265, 1997.

[22] S. Kapuria, S. Sengupta and P. C. Dumir, Three-dimensional solution for a hybrid cylindrical shell under axisymmetric thermoelectric load, *Archive of Applied Mechanics*, vol. 67(5), pp. 320–330, 1997.

[23] E. Carrera, Temperature profile influence on layered plates response considering classical and advanced theories, *AIAA Journal*, vol. 40(9), pp. 1885–1896, 2002.

[24] E. Carrera, An assessment of mixed and classical theories for the thermal stress analysis of orthotropic multilayered plates, *Journal of Thermal Stresses*, vol. 23(9), pp. 797–831, 2000.

[25] A. Robaldo and E. Carrera, Mixed finite elements for thermoelastic analysis of multilayered anisotropic plates, *Journal of Thermal Stresses*, vol. 30, pp. 165–194, 2007.

[26] E. Carrera and A. Robaldo, Extension of Reissner's mixed variational principle to thermopiezoelasticity, *Atti della Accademia delle Scienze di Torino*, vol. 31, pp. 27–42, 2007.

[27] P. Nali, E. Carrera and A. Calvi, Advanced fully coupled thermo-mechanical plate elements for multilayered structures subjected to mechanical and thermal loading, *International Journal for Numerical Methods in Engineering*, vol. 85, pp. 869–919, 2011.

[28] E. Carrera and A. Ciuffreda, Closed-form solutions to assess multilayered-plate theories for various thermal stress problems, *Journal of Thermal Stresses*, vol. 27, pp. 1001–1031, 2004.

[29] E. Carrera, M. Cinefra and F. A. Fazzolari, Some results on thermal stress of layered plates and shells by using Unified Formulation, *Journal of Thermal Stresses*, vol. 36, pp. 589–625, 2013.

[30] S. Brischetto, R. Leetsch, E. Carrera, T. Wallmersperger and B. Kröplin, Thermo-mechanical bending of functionally graded plates, *Journal of Thermal Stresses*, vol. 31(3), pp. 286–308, 2008.

[31] F. A. Fazzolari and E. Carrera, Thermal stability of FGM sandwich plates under various through-the-thickness temperature distributions, *Journal of Thermal Stresses*, vol. 37, pp. 1449–1481, 2014.

[32] S. Brischetto and E. Carrera, Thermal stress analysis by refined multilayered composite shell theories, *Journal of Thermal Stresses*, vol. 32(1-2), pp. 165–186, 2009.

[33] M. Cinefra, E. Carrera, S. Brischetto and S. Belouettar, Thermo-mechanical analysis of functionally graded shells, *Journal of Thermal Stresses*, vol. 33, pp. 942–963, 2010.

[34] A. Robaldo, E. Carrera, and A. Benjeddou, Unified formulation for finite element thermoelastic analysis of multilayered anisotropic composite plates, *Journal of Thermal Stresses*, vol. 28, pp. 1031–1065, 2005.

[35] E, Carrera, Theories and finite elements for multilayered, anisotropic, composite plates and shells, *Archives of Computational Methods in Engineering*, vol. 9(2), pp. 87–140, 2002.

[36] E. Carrera, Theories and finite elements for multilayered plates and shells: a unified compact formulation with numerical assessment and benchmarking, *Archives of Computational Methods in Engineering*, vol. 10(3), pp. 215–296, 2003.

[37] K. J. Bathe, P. S. Lee and J. F. Hiller, Towards improving the MITC9 shell element, *Computers and Structures*, vol. 81, pp. 477–489, 2003.

[38] C. Chinosi and L. Della Croce, Mixed-interpolated elements for thin shell, *Communications in Numerical Methods in Engineering*, vol. 14, pp. 1155–1170, 1998.

[39] N. .C Huang, Membrane locking and assumed strain shell elements, *Computers and Structures*, vol. 27(5), pp. 671–677, 1987.

[40] P. Panasz and K. Wisniewski, Nine-node shell elements with 6 dofs/node based on two-level approximations. Part I theory and linear tests, *Finite Elements in Analysis and Design*, vol. 44, pp. 784–796, 2008.

[41] L. Librescu and W. Lin, Non-linear response of laminated plates and shells to thermomechanical loading: Implications of violation of interlaminar shear traction continuity requirement, *International Journal of Solids and Structures*, vol. 36(27), pp. 4111–4147, 1999.

[42] A. W. Leissa, *Vibration of shells*, NASA National Aeronautics and Space Administration, Washington, DC, SP-288, 1973.

[43] E. Carrera, Multilayered shell theories accounting for layerwise mixed description, Part 1: governing equations, *AIAA Journal*, vol. 37(9), pp. 1107–1116, 1999.

[44] E. Carrera, Multilayered shell theories accounting for layerwise mixed description, Part 2: numerical evaluations, *AIAA Journal*, vol. 37(9), pp. 1117–1124, 1999.

[45] W. T. Koiter, On the foundations of the linear theory of thin elastic shell, *Proc. Kon. Nederl. Akad. Wetensch.*, vol. 73, pp. 169–195, 1970.

[46] P. G. Ciarlet and L. Gratie, Another approach to linear shell theory and a new proof of Korn's inequality on a surface, *Comptes Rendus Mathematique*, vol. 340, pp. 471–478, 2005.

[47] P. M. Naghdi, The theory of shells and plates, *Handbuch der Physic*, vol. 4, pp. 425–640, 1972.

[48] M. Cinefra, E. Carrera, and S. Valvano, Variable Kinematic Shell Elements for the Analysis of Electro-Mechanical Problems, *Mechanics of Advanced Materials and Structures*, vol. 22(1-2), pp. 77–106, 2015.

[49] H. Murakami, Laminated composite plate theory with improved in-plane responses, *Journal of Applied Mechanics*, vol. 53, pp. 661–666, 1986.

[50] K. J. Bathe and E. Dvorkin, A formulation of general shell elements - the use of mixed interpolation of tensorial components, *International Journal for Numerical Methods in Engineering*, vol. 22, pp. 697–722, 1986.

[51] M. L. Bucalem and E. Dvorkin, Higher-order MITC general shell elements, *International Journal for Numerical Methods in Engineering*, vol. 36, pp. 3729–3754, 1993.

[52] M. Cinefra and S. Valvano. A variable kinematic doubly-curved MITC9 shell element for the analysis of laminated composites. *Mechanics of Advanced Materials and Structures*, In Press.

[53] K. Bhaskar, T. K. Varadan and J. S. M. Ali, Thermoelastic solutions for orthotropic and anisotropic composite laminates, *Composites: Part B*, vol. 27(B), pp. 415–420, 1996.

[54] M. Cinefra, C. Chinosi and L. Della Croce, MITC9 shell elements based on refined theories for the analysis of isotropic cylindrical structures, *Mechanics of Advanced Materials and Structures*, vol. 20, pp. 91–100, 2013.

[55] M. Cinefra and E. Carrera, Shell finite elements with different through-the-thickness kinematics for the linear analysis of cylindrical multilayered structures, *International Journal for Numerical Methods in Engineering*, vol. 93, pp. 160–182, 2013.

Tables

Material	Composite	Aluminium	Titanium	Carbon
E_{11}	25.0	$70.3\,E9$	$110.0\,E9$	25.0
E_{22}	1.0	$70.3\,E9$	$110.0\,E9$	1.0
E_{33}	1.0	$70.3\,E9$	$110.0\,E9$	1.0
ν_{12}	0.25	0.33	0.32	0.25
ν_{13}	0.25	0.33	0.32	0.25
ν_{23}	0.25	0.33	0.32	0.25
G_{12}	0.5	$26.429\,E9$	$41.667\,E9$	0.5
G_{13}	0.5	$26.429\,E9$	$41.667\,E9$	0.5
G_{23}	0.2	$26.429\,E9$	$41.667\,E9$	0.2
α_1	1.0	$24.0\,E-6$	$8.6\,E-6$	1.0
α_2	1125.0	$24.0\,E-6$	$8.6\,E-6$	3.0
α_3	1125.0	$24.0\,E-6$	$8.6\,E-6$	3.0

Table 1: Physical data for multilayered plate, cylindrical and spherical shell.

Table 2: Plate with lamination $(0°/90°/0°)$. Transverse displacement $w = w(a/2, b/2) * h_{tot}$ and principal in-plane stress $\sigma_{\alpha\alpha} = \sigma_{\alpha\alpha}(a/2, b/2)$, evaluated at $z = \pm h/2$. Transverse shear stress $\sigma_{\alpha z} = \sigma_{\alpha z}(a, 0)$, evaluated at $z = h/6$.

	a/h	2	10	50	100
w	$3D[53]$	96.79	17.39	10.50	10.26
$\sigma_{\alpha\alpha}$	$3D[53]$	1390	1026	967.5	965.4
$\sigma_{\alpha z}$	$3D[53]$	63.92	60.54	14.07	7.073
	$LW4_a$	96.78	17.39	10.50	10.26
	$LW4$	96.77	17.39	10.50	10.26
	$LW1$	89.23	17.62	11.14	10.91
	$ESLZ3$	94.85	17.37	10.50	10.26
w	$ESL4_a$	98.21	16.90	10.47	10.25
	$ESL4$	98.20	16.90	10.47	10.25
	$ESL2$	83.45	14.96	10.38	10.23
	$FSDT$	41.27	18.33	15.17	15.06
	$LW4$	1392	1029	970.1	968.0
	$LW1$	641.5	906.7	896.2	895.7
	$ESLZ3$	1281	1028	970.1	968.0
$\sigma_{\alpha\alpha}$	$ESL4$	1338	1022	969.7	967.9
	$ESL2$	189.1	870.3	963.0	966.2
	$FSDT$	161.8	1065	1190	1194
	$LW4_a$	63.82	60.54	14.07	7.073
	$LW4$	63.93	60.66	14.10	7.088
	$LW1$	42.54	58.78	13.69	6.883
$\sigma_{\alpha z}$	$ESLZ3$	27.42	52.61	12.45	6.263
	$ESL4_a$	37.25	36.33	8.251	4.143
	$ESL4$	37.30	36.41	8.268	4.152
	$ESL2$	11.58	16.21	3.624	1.819
	$FSDT$	44.48	28.00	6.127	3.073

Table 3: Constant thermal profile. Plate with lamination $(0°/90°/0°)$ and cylindrical and spherical panel with lamination $(0°/90°)$, transverse displacement $w = w(a/2, b/2)$, in-plane stress $\sigma_{\alpha\alpha} = \sigma_{\alpha\alpha}(a/2, b/2)$, transverse shear stress $\sigma_{\alpha z} = \sigma_{\alpha z}(a, 0)$, transverse normal stress $\sigma_{zz} = \sigma_{zz}(a/2, b/2)$. Only for the cylindrical and spherical panel the transverse displacement $w = w\,10$, transverse shear stress $\sigma_{\alpha z} = \sigma_{\alpha z}\,10^2$, transverse normal stress $\sigma_{zz} = \sigma_{zz}\,10^2$.

		Plate			Cylindrical			Spherical	
	a/h	10	100	R/h	10	100		10	100
		$z = h/2$			$z = h/2$			$z = h/2$	
	$LW4_a$	68.754	6.8879		4.9843	1.4408		4.6505	1.9888
	$LW4$	68.753	6.8876		4.9846	1.4409		4.6505	1.9890
	$LW1$	68.783	6.8877		4.8907	1.4232		4.5876	1.9551
	$ESLZ3$	68.839	6.8877		4.9628	1.4366		4.6369	1.9805
w	$ESL4_a$	68.777	6.8879		4.9593	1.4366		4.6312	1.9804
	$ESL4$	68.777	6.8877		4.9596	1.4367		4.6313	1.9806
	$ESL2$	68.839	6.8877		4.9015	1.4273		4.5873	1.9618
	$FSDT$	0.0000	0.0000		4.9736	0.6770		4.4581	1.3244
		$z = h/2$			$z = 0^-$			$z = 0^-$	
	$LW4$	612.81	454.01		2.5036	0.2558		3.4327	0.6358
	$LW1$	567.69	453.56		2.3516	0.1301		3.2901	0.5051
	$ESLZ3$	593.28	453.82		2.7386	0.4523		3.7287	0.8255
$\sigma_{\alpha\alpha}$	$ESL4$	609.56	454.48		2.5096	0.2868		3.4389	0.6595
	$ESL2$	595.93	453.54		2.5005	0.2623		3.4476	0.6400
	$FSDT$	553.43	553.43		3.6316	0.9261		3.6614	1.2794
		$z = h/3$			$z = 0^+$			$z = 0^+$	
	$LW4_a$	30.066	2.6696		6.1495	6.5682		7.5142	5.9752
	$LW4$	30.128	2.6752		6.1582	6.5773		7.5241	5.9833
	$LW1$	29.251	2.6743		5.0680	5.8966		5.6191	5.5013
	$ESLZ3$	26.748	2.4338		4.2012	5.4270		5.0108	4.7507
$\sigma_{\alpha z}$	$ESL4_a$	44.361	4.2101		1.6141	3.2464		1.8457	2.6573
	$ESL4$	44.452	4.2188		1.6161	3.2508		1.8478	2.6607
	$ESL2$	26.728	2.4298		0.4314	2.0210		0.3309	1.5369
	$FSDT$	0.0000	0.0000		0.5730	2.7948		1.7815	2.3323
		$z = 0$			$z = 0^+$			$z = -h/4$	
	$LW4$	3.2666	0.0558		-4.2134	-0.2811		-4.9017	-0.1503
	$LW1$	1.2709	0.0361		-11.732	-2.0980		-3.8270	-0.3264
σ_{zz}	$ESLZ3$	2.4211	0.0481		-5.1615	0.1098		-3.2337	0.1982
	$ESL4$	3.0754	1.1539		-5.4135	-0.3486		-3.9658	-0.1466
	$ESL2$	-0.9299	2.4817	32	-4.3722	-0.7267		-3.3934	-0.1670

Table 4: Cylindrical panel with 1 layer made of isotropic materials Aluminum, $N_l = 1$. Transverse displacement $w = w(a/2, b/2) * 10\, h_{tot}\,/\alpha_{Al}\, a^2 \Delta T$, evaluated along the thickness in $z = 0$. Cylindrical panel with 2 layers made of isotropic materials Aluminum-Titanium, $N_l = 2$. Transverse displacement $w = w(a/2, b/2) * 10\, h_{tot}\,/\alpha_{Al}\, a^2 \Delta T$, evaluated along the thickness in $z = h/4$.

N_l	R_β/h	4	10	100	1000
	$ESL4_a$	-1.0091	0.9468	1.2007	0.1151
	$ESL4$	-1.0091	0.9468	1.2008	0.1151
	$ESL3$	-0.9787	0.9603	1.2008	0.1151
1	$ESL2$	-1.0679	1.9784	1.1995	0.1151
	$ESL1$	1.9502	1.9784	1.8359	0.2189
	$FSDT$	1.9838	1.9818	1.7943	0.1715
	$LW4_a$	0.4002	0.7472	0.7468	0.0325
	$LW4$	0.4001	0.7472	0.7468	0.0326
	$LW3$	0.4242	0.7487	0.7468	0.0326
	$LW2$	0.3998	0.7355	0.7468	0.0326
	$LW1$	0.3512	0.7318	0.8630	0.0487
2	$ESL4_a$	0.4053	0.7386	0.7469	0.0325
	$ESL4$	0.4054	0.7386	0.7469	0.0326
	$ESL3$	0.4142	0.7405	0.7471	0.0326
	$ESL2$	-0.2781	0.5087	0.7466	0.0327
	$ESL1$	1.1306	1.1949	1.1524	0.0957
	$FSDT$	1.2350	1.2673	1.1056	0.0463

Table 5: Cylindrical panel with lamination $(0°/90°)$. Transverse displacement $w = w(a/2, b/2)$, in-plane stress $\sigma_{\alpha\alpha} = \sigma_{\alpha\alpha}(a/2, b/2) * 10$, transverse shear stress $\sigma_{\alpha z} = \sigma_{\alpha z}(a, 0) * 10^2$, transverse normal stress $\sigma_{zz} = \sigma_{zz}(a/2, b/2) * 10^3$. The variables are evaluated at $z = 0$.

	R_β/h	10	50	100	500
	$LW4_a$	0.7450	1.1192	1.1359	1.1412
	$LW4$	0.7450	1.1192	1.1359	1.1412
	$LW1$	0.7712	1.1538	1.1706	1.1759
	$ESLZ3$	0.7454	1.1177	1.1342	1.1396
w	$ESL4_a$	0.7461	1.1194	1.1360	1.1413
	$ESL4$	0.7461	1.1194	1.1360	1.1413
	$ESL2$	0.7455	1.1152	1.1316	1.1369
	$FSDT$	0.8745	1.2781	1.2941	1.2979
	$LW4_a$	0.1802	0.4204	0.3855	0.3446
	$LW4$	0.1805	0.4213	0.3864	0.3454
	$LW1$	2.6963	2.7995	2.7627	2.7235
	$ESLZ3$	0.3280	0.4736	0.4290	0.3807
$\sigma_{\alpha\alpha}$	$ESL4_a$	0.2305	0.4192	0.3823	0.3404
	$ESL4$	0.2309	0.4200	0.3831	0.3411
	$ESL2$	0.2010	0.4247	0.3911	0.3519
	$FSDT$	0.4683	0.7037	0.6587	0.6086
	$LW4_a$	-10.901	-3.7541	-2.8789	-2.2428
	$LW4$	-10.923	-3.7615	-2.8845	-2.2471
	$LW1$	-8.3115	-4.0011	-3.5188	-3.1781
	$ESLZ3$	-10.522	-3.5686	-2.7832	-2.2277
$\sigma_{\alpha z}$	$ESL4_a$	-6.8978	-1.7276	-1.2097	-0.8599
	$ESL4$	-6.9120	-1.7309	-1.2120	-0.8614
	$ESL2$	-5.6195	-1.7814	-1.4294	-1.2006
	$FSDT$	-4.8037	-0.6032	-0.2571	-0.0436
	$LW4_a$	16.981	3.5138	1.9186	0.4215
	$LW4$	17.007	3.5359	1.9369	0.4370
	$LW1$	991.25	913.40	910.39	909.18
σ_{zz}	$ESLZ3$	28.853	2.5312	1.3325	0.2854
	$ESL4_a$	26.667	0.1818	-1.3515	-2.5631
	$ESL4$	26.682	0.1809	-1.3563	-2.5703
	$ESL2$	17.342	-1.3994	-2.2390	-2.8356

Table 6: Spherical panel with lamination $(0°/90°)$. Transverse displacement $w = w(a/2, b/2)$, in-plane stress $\sigma_{\alpha\alpha} = \sigma_{\alpha\alpha}(a/2, b/2) * 10$ and transverse normal stress $\sigma_{zz} = \sigma_{zz}(a/2, b/2) * 10^3$ evaluated at $z = 0$, transverse shear stress $\sigma_{\alpha z} = \sigma_{\alpha z}(a, 0) * 10^2$ evaluated at $z = -h/4$.

|	R/h	10	50	100	500
	$LW4_a$	0.3299	1.0507	1.1174	1.1404
	$LW4$	0.3299	1.0507	1.1174	1.1405
	$LW1$	0.3386	1.0836	1.1516	1.1751
	$ESLZ3$	0.3306	1.0496	1.1159	1.1388
w	$ESL4_a$	0.3309	1.0511	1.1176	1.1406
	$ESL4$	0.3309	1.0511	1.1176	1.1406
	$ESL2$	0.3315	1.0477	1.1134	1.1361
	$FSDT$	0.3927	1.1967	1.2709	1.2965
	$LW4_a$	-25.208^-	10.291^-	11.875^-	11.363^-
	$LW4$	-25.244^-	10.305^-	11.892^-	11.379^-
	$LW1$	-29.322^-	9.5416^-	11.413^-	11.072^-
	$ESLZ3$	-21.884^-	12.316^-	13.447^-	12.579^-
$\sigma_{\alpha\alpha}$	$ESL4_a$	-24.080^-	10.619^-	12.076^-	11.486^-
	$ESL4$	-24.114^-	10.634^-	12.093^-	11.502^-
	$ESL2$	-25.115^-	10.823^-	12.399^-	11.876^-
	$FSDT$	-17.466^-	19.697^-	21.054^-	20.123^-
	$LW4_a$	24.096	1.1199	-1.3854	-2.5674
	$LW4$	24.131	1.1212	-1.3877	-2.5714
	$LW1$	19.500	1.5598	-0.5309	-1.5931
	$ESLZ3$	21.061	2.4154	0.1275	-1.0771
$\sigma_{\alpha z}$	$ESL4_a$	21.281	0.8662	-1.3842	-2.4603
	$ESL4$	21.312	0.8673	-1.3865	-2.4641
	$ESL2$	20.284	3.0723	0.9925	-0.0983
	$FSDT$	21.845	3.9515	1.5581	0.2307
	$LW4_a$	76.657	9.2085	4.3230	0.8525
	$LW4$	76.652	9.2360	4.3451	0.8698
	$LW1$	1100.7	928.03	915.09	909.73
σ_{zz}	$ESLZ3$	98.145	8.8651	3.9948	0.7759
	$ESL4_a$	111.83	6.3462	0.8566	-2.2210
	$ESL4$	111.83	6.3530	0.8569	-2.2255
	$ESL2$	76.502	2.4683	-0.9816	-2.6625

Figures
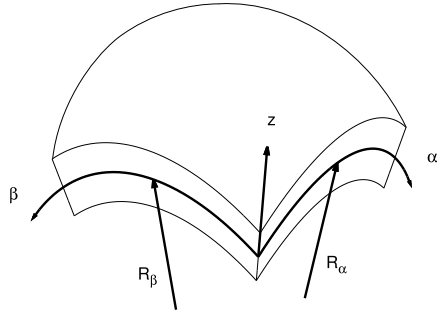
Figure 1: Reference system of the double curvature shell.
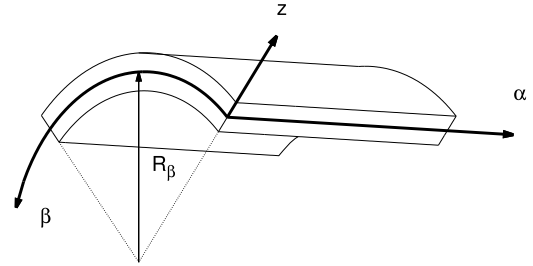
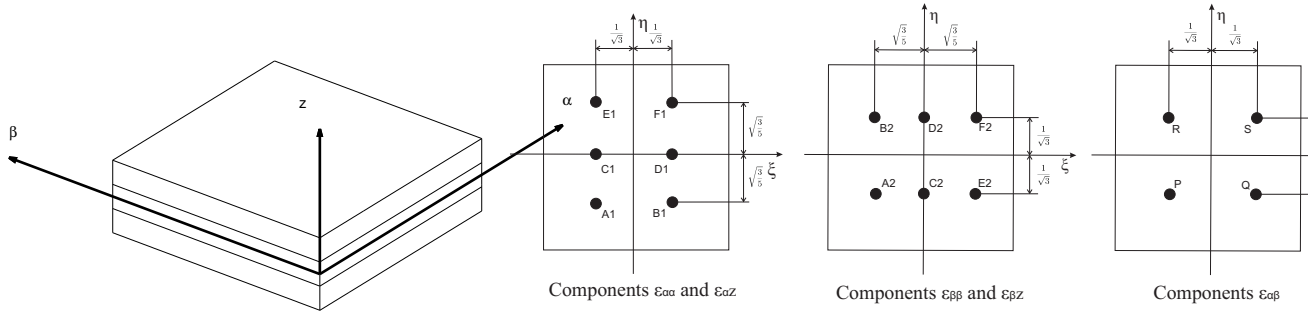Figure 2: Reference system of the cylindrical shell.

Figure 3: Reference system of the plate.

Components $\varepsilon_{\alpha\alpha}$ and $\varepsilon_{\alpha z}$

Components $\varepsilon_{\beta\beta}$ and $\varepsilon_{\beta z}$

Components $\varepsilon_{\alpha\beta}$

Figure 4: Tying points for the MITC9 shell finite element.

36
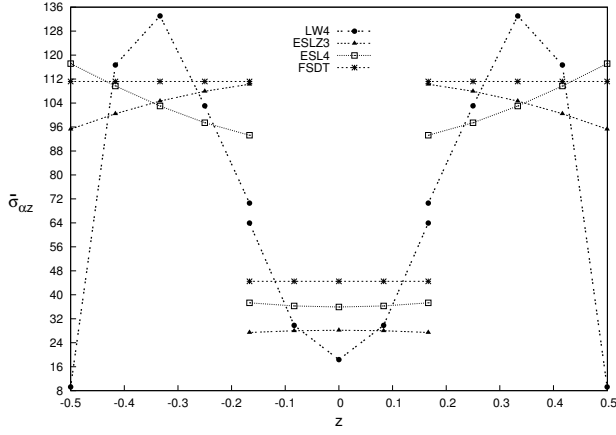
Figure 5: Transverse shear stress $\boldsymbol{\sigma}_{\alpha z}$ along the thickness, with thickness ratio $a/h = 2$. Composite plate.
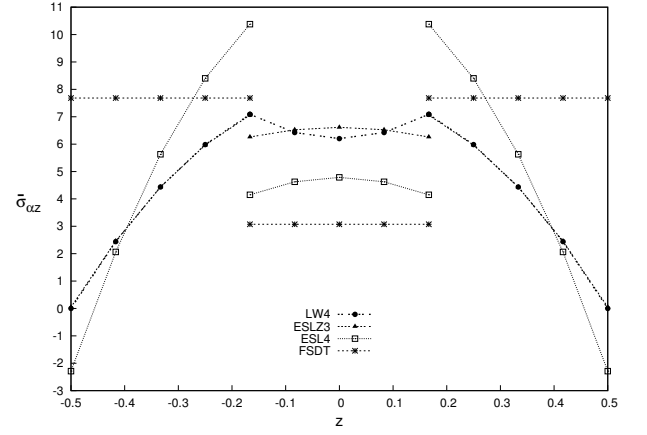
Figure 6: Transverse shear stress $\boldsymbol{\sigma}_{\alpha z}$ along the thickness, with thickness ratio $a/h = 100$. Composite plate.
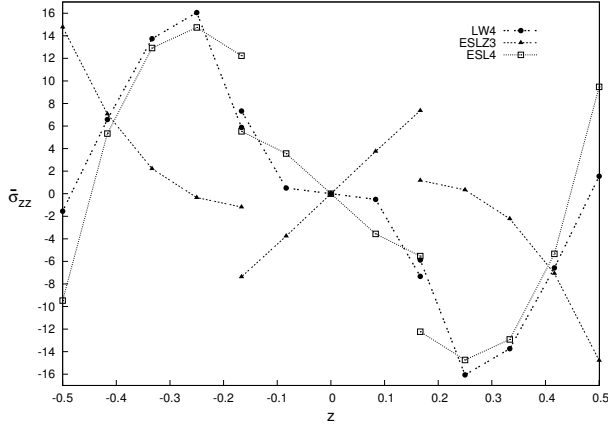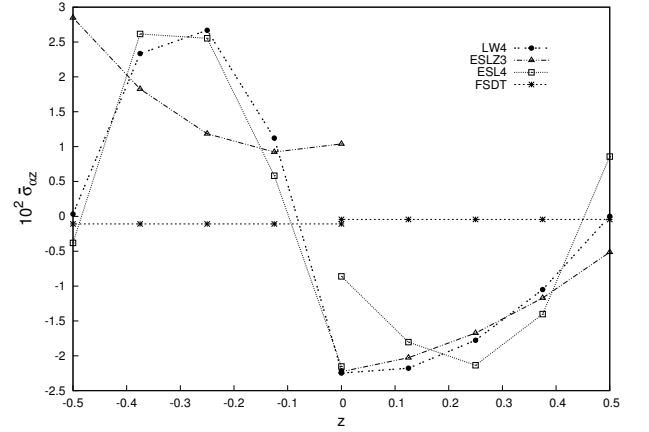

Figure 7: Transverse stress $\boldsymbol{\sigma}_{zz}$ along the thickness, with thickness ratio $a/h = 2$. Composite plate.
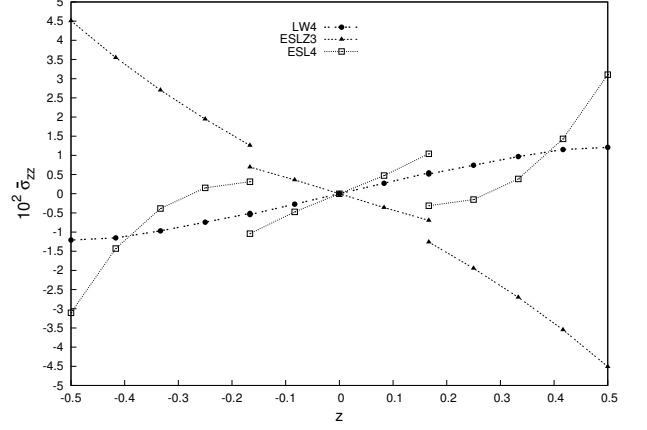
Figure 8: Transverse stress $\boldsymbol{\sigma}_{zz}$ along the thickness, with thickness ratio $a/h = 100$. Composite plate.
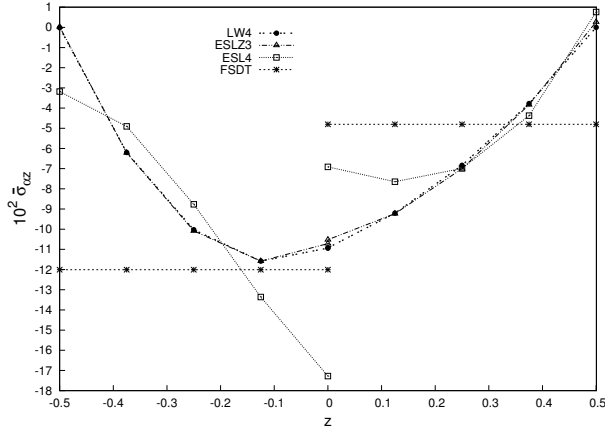
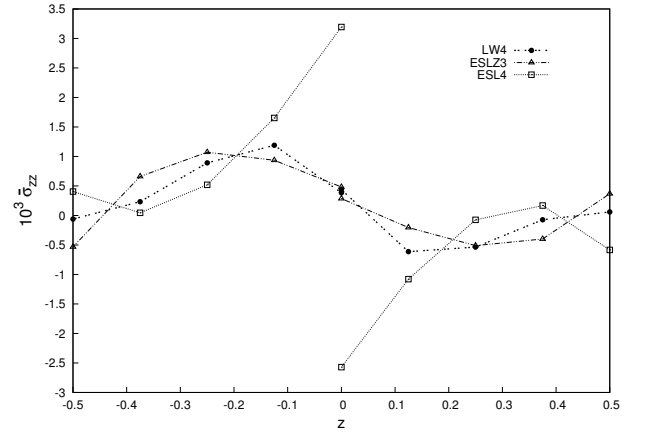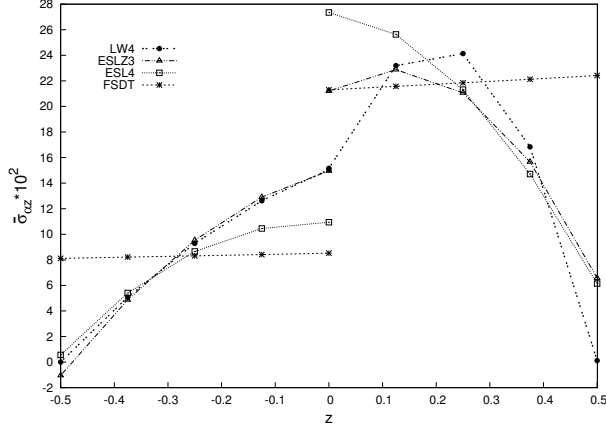Figure 9: Transverse shear stress $\boldsymbol{\sigma}_{\alpha z}$ along the thickness, with thickness ratio $R/h = 10$. Cylindrical composite shell.

Figure 10: Transverse shear stress $\boldsymbol{\sigma}_{\alpha z}$ along the thickness, with thickness ratio $R/h = 500$. Cylindrical composite shell.
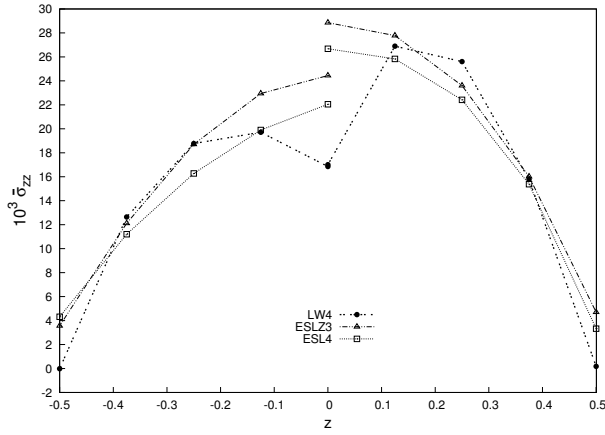
Figure 11: Transverse stress $\boldsymbol{\sigma}_{zz}$ along the thickness, with thickness ratio $R/h = 10$. Cylindrical composite shell.

Figure 12: Transverse stress $\boldsymbol{\sigma}_{zz}$ along the thickness, with thickness ratio $R/h = 500$. Cylindrical composite shell.

Figure 13: Transverse shear stress $\boldsymbol{\sigma}_{\alpha z}$ along the thickness, with thickness ratio $R/h = 10$. Spherical composite shell.
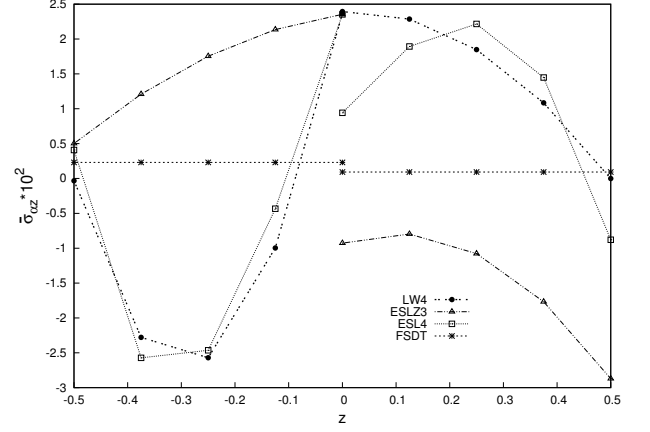

Figure 14: Transverse shear stress $\boldsymbol{\sigma}_{\alpha z}$ along the thickness, with thickness ratio $R/h = 500$. Spherical composite shell.
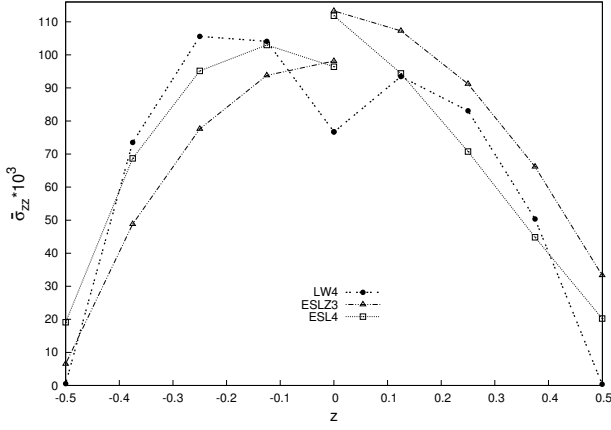

Figure 15: Transverse stress $\boldsymbol{\sigma}_{zz}$ along the thickness, with thickness ratio $R/h = 10$. Spherical composite shell.
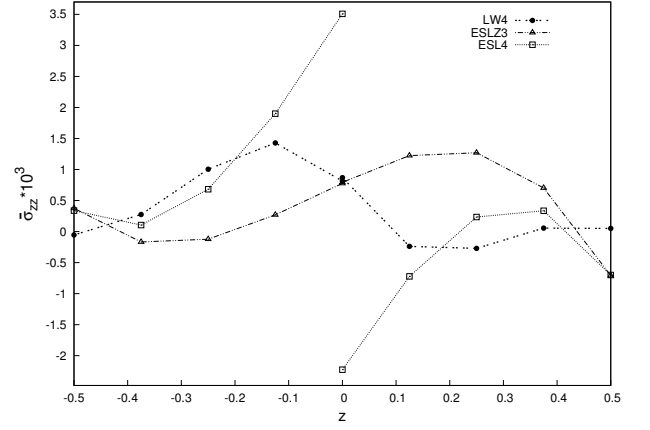

Figure 16: Transverse stress $\boldsymbol{\sigma}_{zz}$ along the thickness, with thickness ratio $R/h = 500$. Spherical composite shell.